Charge-density-wave conduction: Dynamics and finite-size effects

Mark O. Robbins* and R. A. Klemm†
Corporate Research Science Laboratories, Exxon Research and Engineering Company, Clinton Township, Route 22 East, Annandale, New Jersey 08801
(Received 2 December 1985)

The charge-density-wave dynamics in samples with size on the order of a Lee-Rice domain are calculated. At high frequency and current the conductivity approaches that of infinite samples. An explanation for the apparent discrepancy between measurements at large currents and the asymptotic behavior derived by Sneddon, Cross, and Fisher is presented. Finite-size effects change the response at low frequency and current. A kink is introduced in dV/dI near the threshold for dc conduction. Our results agree quantitatively with experiments on some $NbSe_3$ samples. The ac response is found to be substantially broader than the overdamped harmonic-oscillator form which has been used to describe experimental results. The response is characteristic of a distribution of relaxation times similar to that observed in recent experiments. This distribution is related to the elastic modes of the deformable charge-density-wave condensate. A relation between the frequency and current dependence of the damping by these modes is derived. Our results are compared with those for infinite samples.

I. INTRODUCTION

In recent years a new mechanism of conductivity, charge-density-wave (CDW) conduction, has been discovered and extensively investigated.[1] The CDW condensate forms below the Peierls transition temperature T_P. At low dc electric fields the CDW condensate is pinned by its interaction with impurities, but above a threshold field E_T the condensate is depinned and contributes to the conductivity. This leads to a highly nonlinear dc conductivity and a wealth of other interesting phenomena. At dc biases above the threshold for nonlinearity, periodic voltage oscillations (narrow-band noise) and $1/f$ noise occur.[2] The ac conductivity shows strong frequency dependence which is similar to the field dependence of the dc conductivity.[3] A broad distribution of relaxation times is seen in both the ac conductivity[4] and the $1/f$ noise.[5] A variety of phenomena with very long timescales have been observed: hysteresis in the current-voltage (I-V) characteristic,[6,7] relaxation after applied pulses,[7,8] and switching.[6]

A variety of models have been proposed for CDW conduction based on both classical[1,9-11] and quantum[12] pictures. In this paper we investigate a classical model based on the perturbation method developed by Klemm and Schrieffer[11] (KS) for pinning by weak impurities. The major improvement over previous work based on this approach[11] is that damping by the internal elastic modes of the CDW is included. This has a dramatic effect on the ac and dc response.

The perturbation approach is only convergent for sufficiently small samples. However, it is important to understand CDW dynamics on these length scales for several reasons. One reason is that such small sample sizes are experimentally realizable. Another is that theories for infinite samples often proceed by coupling small regions together. The internal dynamics of these regions must be included properly in a complete theory. Finally, calculations for small samples give several direct insights into the response of infinite samples. For example, on short timescales (high frequencies and currents) the response of small samples approaches that of infinite samples. Our model gives the asymptotic high-field dependence of the dc conductivity derived by Sneddon, Cross, and Fisher[13] (SCF), $\sigma \sim \sigma_\infty - cE^{-1/2}$. It also gives the leading corrections to the SCF behavior and provides an explanation for the apparent disagreement reported[14] with experiment. On long timescales, finite-size effects become important and our model indicates how these affect the CDW response. In particular, we find a "kink" in dV/dI near E_T similar to that observed experimentally in some samples.[15]

The form of the high-field dc conductivity results from a current dependent damping rate due to damping by internal elastic modes. We find that the damping rate for the ac conductivity has the same form as a function of frequency. This frequency-dependent damping rate corresponds to a broad distribution of relaxation times similar to that observed in experiments.[4,5] Finite-size effects cut off the distribution at long relaxation times. There are several important experimental consequences of this distribution of relaxation times: the response becomes substantially broader, the imaginary parts of the ac conductivity and dielectric function peak at different frequencies, and the peak positions vary with dc bias in different ways. Experiments are consistent with all of these results.

In the next section we describe the perturbation theory used for our calculations and discuss its structure qualitatively. In Sec. III we present results for the dc and ac conductivities. Conclusions and other implications for experimental behavior are presented in the final section.

II. TIME-DEPENDENT PERTURBATION THEORY

Experiments on CDW systems indicate that the amplitude of the CDW order parameter is field independent,[16]

and that changes in the phase of the order parameter $\phi(\mathbf{r},t)$ are overdamped.[17–19] Thus the classical equation of motion for $\phi(\mathbf{r},t)$ is written as[9–11]

$$\left[\tau_0^{-1}\frac{\partial}{\partial t}-\nabla^2\right]\phi=e^*E+V_0\,\delta n(\mathbf{r})\sin(\mathbf{Q}\cdot\mathbf{r}+\phi)\ , \tag{1}$$

where lengths have been scaled to make the equation isotropic and the velocity of phase excitations is set equal to 1. The terms on the left-hand side of Eq. (1) are the damping force and the elastic force which limits distortions of the CDW. The terms on the right-hand side are the effective coupling to the component E of the electric field along the CDW wave vector $\mathbf{Q}$, and the pinning force due to impurities with concentration c, local density $\delta n(\mathbf{r})$, and pinning strength V_0. The experimentally measured CDW current will be proportional to the time derivative of the collective coordinate Δ, defined as the volume average of ϕ.

Two distinct pinning regimes have been identified.[9] For $V_0>c^{-1/3}$ or $V_0>\lambda$, where λ is the coherence length for the CDW amplitude, there is strong pinning: the CDW deforms to optimize the phase at each impurity. We consider the case of weak pinning, $V_0<c^{-1/3}$ and $V_0<\lambda$, where the phase can no longer be optimized at each site. It varies on the scale of the static phase coherence length, or Lee-Rice domain size,[9] $\xi=16\pi/cV_0^2$, to conform to fluctuations in the pinning potential of many impurities.[10] Thus for samples with dimension $L<\xi$, the spatial fluctuation in the phase, $\delta\phi(\mathbf{r},t)\equiv\phi(\mathbf{r},t)-\Delta(t)$, is a small parameter which may be treated either perturbatively or iteratively.

We consider a cubic sample of side L with periodic boundary conditions. Then taking the average of Eq. (1) over volume $\Omega=L^3$ yields

$$\tau_0^{-1}\dot{\Delta}(t)=e^*E(t)+V_0\langle\delta n(\mathbf{r})\sin[\mathbf{Q}\cdot\mathbf{r}+\Delta(t)+\delta\phi(\mathbf{r},t)]\rangle_\Omega\ . \tag{2}$$

The equation for $\delta\phi$ can be written as

$$\delta\phi(\mathbf{r},t)=\int_\Omega d\mathbf{r}'\,dt'\,G(\mathbf{r}-\mathbf{r}',t-t')V_0\,\delta n(\mathbf{r}')\times\sin[\mathbf{Q}\cdot\mathbf{r}'+\Delta(t')+\delta\phi(\mathbf{r}',t')]\ , \tag{3}$$

where the Green's function G satisfies

$$\left[\tau_0^{-1}\frac{\partial}{\partial t}-\nabla^2\right]G=\delta(\mathbf{r})\delta(t)\ , \tag{4}$$

periodic boundary conditions, and has zero spatial average. The solution satisfying these conditions is

$$G(\mathbf{r},t)=\frac{1}{2\pi\Omega}\int d\omega\sum_{\mathbf{K}\,(\neq0)}(K^2+i\omega\tau_0^{-1})^{-1}e^{i(\omega t-\mathbf{K}\cdot\mathbf{r})}\ , \tag{5}$$

where the sum is over the reciprocal-lattice vectors: $\mathbf{K}=(h\hat{\mathbf{x}}+k\hat{\mathbf{y}}+l\hat{\mathbf{z}})2\pi/L$, with h, k, and l any integers.

Equation (4) describes diffusive transport. There is thus a natural timescale $t_L\equiv L^2/\tau_0$: the time for diffusive propagation of phase excitations (phasons) across the sample. It can be shown that the response of a finite sample approaches that of an infinite sample for processes with timescales less than t_L, i.e., for ac fields with $\omega\gg2\pi/t_L$, or dc currents where $\dot{\Delta}\gg2\pi/t_L$. Therefore calculations for samples with $L<\xi$ reveal the response characteristic of large samples on short timescales as well as indicating how finite-size effects may be important on longer timescales.

If $\delta\phi\ll2\pi$, Eqs. (2) and (3) may be solved perturbatively. To check this criterion we have calculated $\langle|\delta\phi|^2\rangle_{\Omega\alpha}$, the mean-squared value of $\delta\phi$ averaged over volume and impurity configurations, α, to lowest order. Setting $\delta\phi$ equal to zero on the right-hand side of Eq. (3), and using

$$\langle\delta n(\mathbf{r})\delta n(\mathbf{r}')\rangle_\alpha=c\delta(\mathbf{r}-\mathbf{r}')$$

for uncorrelated impurities, we find

$$\langle|\delta\phi|^2\rangle_\alpha=cV_0^2\int d\mathbf{r}\int dt\int dt'\,G(\mathbf{r},t)G(\mathbf{r},t')\times\sin[\mathbf{Q}\cdot\mathbf{r}+\Delta(t)]\times\sin[\mathbf{Q}\cdot\mathbf{r}+\Delta(t')]\ . \tag{6}$$

The maximum value occurs for a static system, $\Delta(t)=\Delta(t')$. In this case the integrals over time just pick out the $\omega=0$ component of G, and

$$\langle|\delta\phi|^2\rangle_\alpha=(2\pi)^2\eta LcV_0^2\ ,$$

with

$$\eta=(1/8\pi^2)\sum_{\mathbf{K}(\neq0)}(KL)^{-4}\simeq1.3\times10^{-4}\ .$$

Thus the perturbation expansion is valid when $L\ll\xi'\equiv1/(\eta cV_0^2)\simeq148\xi$. At high frequencies and currents $\langle|\delta\phi|^2\rangle_\alpha$ decreases, $\langle|\delta\phi|^2\rangle_\alpha\propto\dot{\Delta}^{-1/2}$ for $\dot{\Delta}t_L\gg1$, and the accuracy of the perturbation approach improves.

In this paper we consider small samples $L<\xi'$ and therefore only include $\delta\phi$ to the lowest nontrivial order. An approximate value for $\delta\phi$ is obtained from Eq. (3) with $\delta\phi$ set equal to zero on the right-hand side. This approximate value is then included to first order in Eq. (2). The resulting equation for Δ is

$$\dot{\Delta}(t)=F(t)+\mathrm{Im}\{Ae^{i\Delta(t)}+\int dt'[B^+(t-t')e^{i[\Delta(t')+\Delta(t)]}+B^-(t-t')e^{i[\Delta(t')-\Delta(t)]}]\}\ , \tag{7}$$

where time and length are measured in units of t_L and L, $F\equiv L^2e^*E$, and A and B are dimensionless functions of the particular arrangement of impurities:

$$A\equiv(V_0/L)\int_\Omega d\mathbf{r}\,e^{i\mathbf{Q}\cdot\mathbf{r}}\delta n(\mathbf{r}) \tag{8}$$

$$B^\pm(t)\equiv(V_0^2/2L)\int_\Omega d\mathbf{r}\int_\Omega d\mathbf{r}'\,\delta n(\mathbf{r})G(\mathbf{r}-\mathbf{r}',t)\delta n(\mathbf{r}')\times e^{i\mathbf{Q}\cdot(\mathbf{r}'\pm\mathbf{r})}\ . \tag{9}$$

Note that the phase at previous times enters explicitly in the equation of motion for the CDW current, suggesting how hysteresis[6,7] and memory effects[7,8] enter naturally into the problem.

Information about A and $B^{\pm}$ can be obtained by calculating their moments averaged over impurity configurations, α. As mentioned above, pinning by weak impurities arises from fluctuations in the impurity potential. The coefficients A and B^{+} reflect these fluctuations and their average over impurity configurations vanishes. However, their average amplitudes are nonzero:

$$\langle |A|^2\rangle_\alpha=(L/\eta\xi'), \tag{10}$$

$$\langle |B^{+}(t)|^2\rangle_\alpha=0.5(L/\eta\xi')^2\int_\Omega d\mathbf{r}\,|G(\mathbf{r},t)|^2/L . \tag{11}$$

In contrast, the impurity average of B^{-} is nonzero,

$$\langle B^{-}(t)\rangle_\alpha=(L/2\eta\xi')LG(0,t) . \tag{12}$$

This term comes from successive scatterings by the same site. Fluctuations about this mean value,

$$\langle |B^{-}(t)-\langle B^{-}(t)\rangle|^2\rangle_\alpha=0.5\langle |B^{+}(t)|^2\rangle_\alpha , \tag{13}$$

are small compared to $\langle B^{-}\rangle_\alpha$ because the maximum value of G is always at $r=0$. The importance of the role played by B^{-} is described below.

Klemm and Schrieffer[11] (KS) have studied Eq. (7) in the static limit, making the adiabatic approximation $\Delta(t')=\Delta(t)$ on the right-hand side. This provides a microscopic derivation of an equation of motion similar to that suggested by Grüner, Zawadowski, and Chaikin[17] (GZC) for a rigid, overdamped CDW. The collective coordinate Δ acts like an overdamped particle moving in an effective periodic potential. Indeed, in the limit $L/\xi'\to 0$, $B^{\pm}$ become unimportant and the effective periodic potential becomes sinusoidal as assumed by GZC. Both $B^{\pm}$ represent the effect of internal deformations of ϕ in response to the impurity potential. The response increases as L/ξ' increases and the periodic potential becomes more highly structured. For example, the second harmonic of the potential is $0.5\int dt\,B^{+}(t)$, which increases relative to A as $(L/\xi')^{1/2}$. Klemm and Schrieffer showed that the increased structure in the periodic potential for Δ affects the narrrow-band noise spectrum and other properties.

The full equation of motion [Eq. (7)] also yields an effective periodic potential, which is identical to the KS result for slow processes. However, the internal deformations which determine this potential produce other important effects which are not included in the adiabatic approximation: The periodic potential becomes current and frequency dependent, the system acquires memory, and the internal deformations contribute to the rate of dissipation. As shown below, this dissipation plays a crucial role in determining the field and frequency dependence of the conductivity.

In fact, the CDW *never* moves adiabatically. For a constant field experiment, $\dot{\Delta}$ will have magnitudes as large as $2|A|\sim 200(L/\xi')^{1/2}$ as Δ varies through 2π—the phase changes rapidly compared to the time t_L for information to traverse the sample. A more surprising result is that for arbitrarily small constant CDW current the damping rate τ_0^{-1} is renormalized. This renormalization varies with $\dot{\Delta}$ in a way that fundamentally alters the field dependence of the conductivity from the GZC result.

For a constant current, we may replace $\Delta(t)$ by $\Delta_0+\dot{\Delta}t$ in Eq. (7). The terms from A and B^{+} oscillate, yielding periodic voltage oscillations. In contrast, the contribution from the B^{-} term is a constant, $b^{-}(\dot{\Delta})$, the Fourier transform of $B^{-}(t)$. The result is an effective renormalization of the damping rate to

$$\tau^{-1}(\dot{\Delta})=\tau_0^{-1}\{1-\mathrm{Im}[b^{-}(\dot{\Delta})]/\dot{\Delta}\} . \tag{14}$$

The dominant contribution to b^{-} comes from $\langle B^{-}\rangle_\alpha$, which is due to double scattering by each site, and represents a Born approximation for the damping of the CDW through phason excitations at each impurity. Note that in the adiabatic approximation the contribution from B^{-} is identically zero because B^{-} is real by symmetry.

The behavior of $\tau^{-1}(\dot{\Delta})/\tau_0^{-1}$ is illustrated in Fig. 1 for several values of L/ξ'. The case $L/\xi'=0$ corresponds to the rigid CDW model;[17] τ^{-1} is constant. In the limit $\omega\ll t_L^{-1}$ each term in the sum of Eq. (5) may be approximated by $K^{-2}(1-i\omega t_L(LK)^{-2})$. Taking the imaginary part and combining Eqs. (12) and (14), we find that the damping rate approaches a constant,

$$\tau^{-1}(\dot{\Delta})/\tau_0^{-1}=1+(2\pi)^2L/\xi' .$$

For $\dot{\Delta}\gg t_L^{-1}$ the sum in Eq. (5) may be approximated by an integral over $\mathbf{K}$. This gives

$$[\tau^{-1}(\dot{\Delta})/\tau_0^{-1}-1]\propto(L/\xi')(\dot{\Delta}t_L)^{-1/2} .$$

The physics underlying this variation of the damping rate is easily understood. The increase relative to τ_0^{-1} comes from dissipation through excitations of internal deformations or phasons. For slow processes, the damping rate is constant because of finite-size effects. The lowest phason frequency is of order $\omega_L\equiv(2\pi)^2t_L^{-1}$. When $\dot{\Delta}\ll\omega_L$ all phasons are excited and contribute to the damping rate. As the current increases, $\dot{\Delta}>\omega_L$, the lower-frequency phasons in the moving frame of the CDW cannot respond to the rapidly varying impurity potential. The damping rate decreases. This physical interpretation of the decrease in damping is borne out by the behavior of $\langle |\delta\phi|^2\rangle_\alpha$ as a function of $\dot{\Delta}$, which was described above. The amplitude of phase fluctuations,

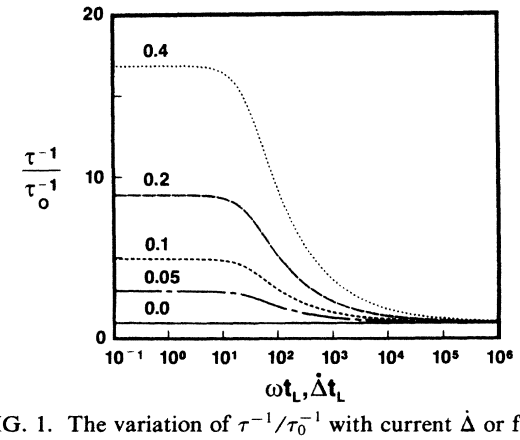

FIG. 1. The variation of τ^{-1}/τ_0^{-1} with current $\dot{\Delta}$ or frequency ω is illustrated for the indicated values of L/ξ'. The case $L/\xi'=0$ corresponds to the rigid CDW model where τ^{-1} is a constant.

which reflects the response of the CDW to the impurities, decreases monotonically as $\dot{\Delta}$ increases. The contributions to the periodic potential from internal deformations (e.g., B^+) also decrease.

An important result is that the same renormalized damping rate enters into the ac conductivity. The linear ac response at a dc bias $\tilde{E}$ below threshold is calculated from Eq. (7) by expanding about the static phase $\tilde{\Delta}$ in zero ac field. One finds (see Appendix)

$$\sigma(\omega)=[\tau^{-1}(\omega)-i\omega^{-1}K(\omega)]^{-1}\ , \tag{15}$$

with τ^{-1} given by Eq. (14) with $\dot{\Delta}$ replaced by ω, and

$$K(\omega)\equiv\tilde{K}+\{b^+(\tilde{\Delta},0)-b^+(\tilde{\Delta},\omega)+\mathrm{Re}[b^-(0)-b^-(\omega)]\}\ . \tag{16}$$

Here, $\tilde{K}$ is the force constant for small static displacements about $\tilde{\Delta}$, and $b^+(\tilde{\Delta},\omega)$ is the Fourier transform of the real part of $\exp(2i\tilde{\Delta})B^+(t)$.

As described above, the damping rate is determined by the response of the phasons. The main factor determining a phason's response is the ratio of its frequency to the characteristic frequency of the motion. At constant dc current the impurities "see" an oscillating phase with $\omega=\dot{\Delta}$. The contribution of phasons to damping is the same as when an external field drives the CDW phase with the same ω. In our units, the scaling factor between ω and $\dot{\Delta}$ is unity. It is readily determined experimentally by measuring the ratio of the CDW current to the narrow-band noise frequency or Shapiro step frequency.[1]

A frequency-dependent damping rate is often interpreted in terms of a distribution of relaxation times.[4] In our model this distribution corresponds to the distribution of phasons with the relaxation time for each given by the inverse of its frequency. The implications for the form of the ac response are described in detail in Sec. III C.

III. RESULTS

A. dc response near threshold

Equation (7) was solved numerically at constant field and the mean current was evaluated over timescales much longer than both t_L and the characteristic period of motion in the periodic potential. Values of A and $B^{\pm}$ were obtained in two different ways. For the results shown in Figs. 2–7, A and $B^{\pm}$ were calculated from the configuration averages of their moments [Eqs. (10)–(13)]. Values were also obtained by explicit summation of Eqs. (8) and (9) for specific randomly generated impurity distributions. Variations of A and B^+ with impurity configuration change the value of the threshold field and the precise form of the effective periodic potential. Higher order terms in perturbation theory than those included in Eq. (7) would produce similar changes. However, when the field is normalized to E_T, the results for the dc response calculated with different choices of A and $B^{\pm}$ for the same sample size are indistinguishable on the scale of Fig. 2. The dominant factor in this plot is the renormalization of τ^{-1}, which has a well-defined configuration average. Fluctuations about this value are small. The results shown are thus very representative of a given sample size and should not change significantly if higher-order terms in perturbation theory are included.

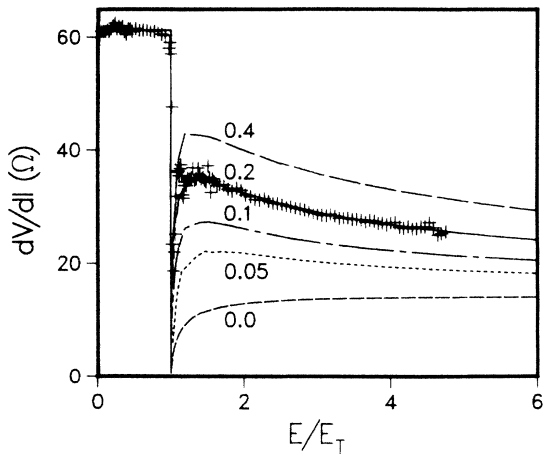

FIG. 2. Differential resistance vs field calculated for the leading values of L/ξ' (curves), and experimental results for $NbSe_3$ at 48 K (pluses). For $L/\xi'=0$ the results are equivalent to the rigid CDW model.

In Fig. 2 the differential resistance is plotted as a function of dc field for several sample sizes. The large field limit of the CDW conductivity σ_∞ is the same for each curve. For comparison with experiment a parallel conductance σ_n due to conduction by normal electrons has been included.

For all sample sizes there is a kink near threshold in dV/dI—a sharp drop followed by a rapid rise. This is the region where the damping rate is constant because of the finite-size cutoff in the phason spectrum. The width of the kink decreases as the sample size increases and the phason frequency cutoff ω_L decreases. The GZC model corresponds to the limit $L/\xi'\to 0$, where τ^{-1} is constant for all E. In this limit the value of dV/dI increases monotonically above E_T. This behavior is never seen experimentally. Instead, dV/dI is found to decrease monotonically at large fields. All curves for $L/\xi'>0$ show this behavior. The decrease reflects the decrease in τ^{-1} (Fig. 1) as fewer and fewer phasons contribute to the damping. The large-field behavior is discussed in detail below.

Also shown in Fig. 2 are experimental results[20] for a 2 mm$\times$10μm$\times$10μm sample of $NbSe_3$ at 48 K. The agreement with theoretical results for $L/\xi'=0.2$ is excellent. The only parameters in the fit other than L/ξ' are σ_n and σ_∞, which merely fix the endpoints of the curve, not the shape. The fit is somewhat less sensitive to sample size than Fig. 1 suggests because σ_∞ is not known for the experimental system. If this asymptotic value is adjusted, the results for $L/\xi'=0.4$ also fit the experimental results fairly well over the measured range of fields, but the overall rise in dV/dI is too large. The best fit would be for a value of L/ξ' slightly larger than 0.2.

In many samples the differential resistivity decreases monotonically above threshold—there is no kink.[15] To date, no explanation for the sample dependence of the threshold behavior has been established.[21] Our calculation suggests that the kink is a finite-size effect. The width of

the kink decreases as L/ξ' increases in Fig. 2 because the finite-size-induced low-frequency cutoff ω_L decreases. Experimentally, kinks in dV/dI tend to correlate with small sample size and low temperature,[15,22] but systematic experiments with varying sample size and coherence length are needed to establish this explanation.

A finite low-frequency cutoff in the phason spectrum will always[23] lead to a kink in dV/dI at threshold, although it may become unmeasurably small. For $L \gg \xi'$, where our perturbation theory is not valid, the value of ω_L at $E=0$ approaches[9] a constant proportional to E_T. However, as E increases towards E_T, $\omega_L \to 0$. For $E > E_T$, the presence of impurities should only affect the phason spectrum of the sliding CDW for frequencies lower than the characteristic frequencies of the CDW motion, which go to zero at threshold. As described above, it is only the modes whose frequencies are higher than those of the motion which renormalize τ^{-1}. We can thus calculate the approximate threshold behavior of an infinite sample by using the phason spectrum of a completely unpinned CDW. The effective damping rate then has the form $\tau^{-1} \propto \dot{\Delta}^{-1/2}$ for all $\dot{\Delta}$. The divergence of τ^{-1} at threshold removes the kink in dV/dI and $I \propto (E-E_T)^{3/2}$ near threshold. This is in qualitative agreement with experiments on large samples;[15] however, reported exponents[24,25] vary from 1.1 to 4. Mean-field scaling treatments[26,27] also give exponents in this range. Although the details of these calculations are very different, there, as here, the threshold behavior is controlled by the very-low-frequency elastic modes.

B. dc response at large fields

Sneddon, Cross, and Fisher[13] showed that the asymptotic form for the dc conductivity is $\sigma \simeq \sigma_\infty - CE^{-1/2}$, and suggested that a plot of the experimental conductivity versus $E^{-1/2}$ should produce a straight line. However, such plots, in general, show a pronounced upward curvature. Sneddon[14] has suggested that this discrepancy is due to the effect of screening by normal electrons, which was not included in the equation of motion [Eq. (1)]. However, we show below that *even in the absence of screening*, plots of σ vs $E^{-1/2}$ show pronounced curvature.

In Fig. 3(a) we present plots of σ/σ_∞ vs $(E/E_T)^{-1/2}$ for the same set of sample sizes and coefficients, A and $B^{\pm}$, used for Fig. 2. The conductivity due to the normal electrons, σ_n, has been subtracted. The results plotted here are more sensitive to the coefficients A and $B^{\pm}$ than those plotted in Fig. 2. While the qualitative features remain unchanged, the height of the initial rise in σ at threshold varies by a factor of ~ 2 as the value of E_T varies. In plots of dV/dI this variation manifests itself in small changes in the shape of the "kink." Unlike σ, dV/dI reflects the local character of the I-V characteristic; thus these changes do not affect results at larger fields. In Fig. 3(a) each curve is normalized to a different threshold field. When plotted in the same units, each curve approaches the results for larger samples for fields larger than about $2E_T$. This is a consequence of the independence of high-field results on sample size discussed above.

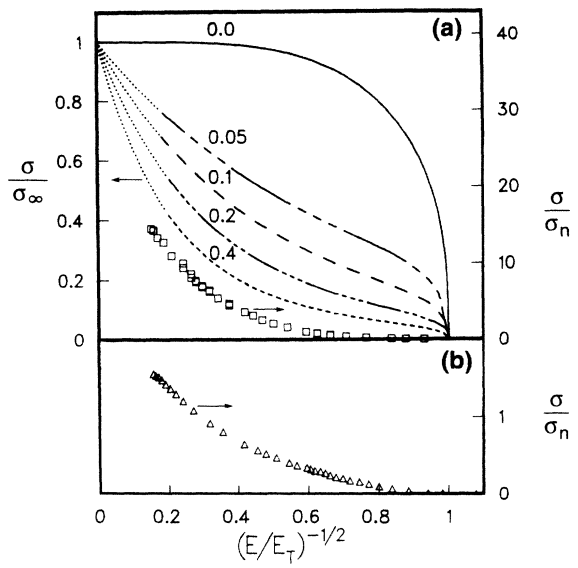

FIG. 3. Plots of the dc CDW conductivity σ vs $(E/E_T)^{-1/2}$. Calculated results for the indicated values of L/ξ' and measurements (squares) on TaS_3 at 150 K are shown in (a), and measurements on $NbSe_3$ at 42 K (triangles) are plotted in (b). The dotted portions of the calculated curves are extrapolations of the data to infinite field using the asymptotic form given in the text.

Near threshold in Fig. 3(a), one sees the effect of the constant damping region introduced by finite-size effects. Results for all sample sizes show a sharp rise in conductivity near threshold with downward curvature. For the GZC model, $L/\xi'=0$, this curvature continues for all fields: $\sigma \sim \sigma_\infty - CE^{-2}$ at high fields. For all other values of L/ξ' the curvature changes sign at values of $(E_T/E)^{-1/2}$ slightly less than 1, as the decrease in τ^{-1} becomes important. This upward curvature is pronounced, and continues to the highest fields studied. It sets in at lower values of σ/σ_α as the sample size increases.

As mentioned above, our calculation gives the same asymptotic high-field behavior as that of Sneddon, Cross, and Fisher.[13] The source of this behavior is the decrease of τ^{-1} at high currents, $\tau^{-1} \simeq \tau_0^{-1} + c\dot{\Delta}^{-1/2}$, which implies $\sigma^{-1} = \sigma_\infty^{-1} + c' I^{-1/2}$. Inverting this relation and replacing I with E, we find

$$\sigma \sim \sigma_\infty [1 - C'x + 0.5(C'x)^2 - \mathcal{O}(x^3)] ,$$

where $x \equiv E^{-1/2}$. The reason that the curves in Fig. 3(a) are not straight lines is that the leading correction to the SCF result is of order E^{-1}. This quadratic term in $E^{-1/2}$ yields a substantial curvature in plots of σ vs $E^{-1/2}$ even in the limit $E^{-1/2} \to 0$. Corrections to the leading order (SCF) result are emphasized in such plots because all of the high-field region is compressed into a small area. If one plots R vs $I^{-1/2}$, there is no term of order I^{-1}, so the curvature goes to zero in the limit $I^{-1/2} \to 0$. However, corrections to R of higher order in $I^{-1/2}$ are present, and these cause noticeable curvature out to the largest currents typically measured.

Also shown in Fig. 3(a) are measurements[22] of the CDW conductivity σ in TaS_3 at 130 K, which extend to

about $50E_T$. The ratio of σ to σ_n is indicated to the right of the figure. The scale relative to the theoretical results is consistent with the value of σ_∞ obtained by extrapolating plots of R vs $I^{-1/2}$ to infinite current. The upward curvature starts immediately at threshold and continues to the highest fields measured. The form of the curve is just what one would expect from an extrapolation of the trend in our calculated results to infinite-length samples. Results for samples with kinked dV/dI curves, like the $NbSe_3$ sample on which the data for Fig. 2 were taken, look like the calculated results for finite size in Fig. 3(a).

Figure 3(b) shows that $NbSe_3$ samples which do not have kinks exhibit high-field behavior very similar to that observed in TaS_3. If screening was important in determining the shape of these curves, as suggested by Sneddon,[14] some variation would be expected. In particular, TaS_3—which is a semiconductor—and $NbSe_3$—which is metallic—should have different degrees of screening.

At extremely high fields neither our calculation nor that of SCF is applicable because inertial terms in the equation of motion [Eq. (1)] have been neglected. Recent ac measurements[18] on TaS_3 and $NbSe_3$ show that inertial effects become important at frequencies above a few GHz. Thus at dc currents corresponding to narrow-band noise frequencies of this magnitude, the high-field behavior will change, reflecting inertial effects. The initial effect will be to decrease the rate of rise of σ. A rough estimate based on measured I-V characteristics and ratios of the CDW current to the narrow-band noise frequency suggests that this should occur at fields of order $100E_T$. Inertial effects may therefore be entering at the highest fields plotted in Fig. 3. Future experimental measurements where the narrow-band noise frequency, dc conductivity, and high-frequency ac conductivity are correlated for a single sample would play an important role in determining the effect of inertial terms on the high-field conductivity.

C. ac conductivity

The variation of the damping rate, which dominates the high-field dc behavior, also changes the ac response dramatically. The linear ac response is given by Eqs. (15) and (16). Figures 4(a) and 4(b) show the real and imaginary parts, σ' and σ'', of the ac conductivity at zero dc bias as a function of ωt_L for different sample sizes. Figures 5(a) and 5(b) show the real and imaginary parts, ϵ' and ϵ'', of the corresponding dielectric function, $\epsilon(\omega)=i\sigma(\omega)/\omega$. As above, values for $\tilde{K}$, b^-, and b^+ were calculated from their moments averaged over impurity positions. Note that in our normalized units the limiting high-frequency conductivity $\sigma(\infty)=1$.

As $L/\xi \to 0$, $b^{\pm} \to 0$, and τ and K in Eq. (15) become frequency independent. The response approaches that predicted by the rigid CDW model,[17] which is identical to that of an overdamped harmonic oscillator (OHO). This response is illustrated in Figs. 4 and 5 for a characteristic crossover frequency,[28] $\omega_c \equiv \tilde{K}\tau$, of $10t_L^{-1}$. The asymptotic response for low and high frequencies is

$$\mathrm{Re}[\sigma(\omega)] \propto \omega^2, \quad \mathrm{Im}[\sigma(\omega)] \propto \omega \quad \text{for } \omega \ll \omega_c \ , \tag{17}$$

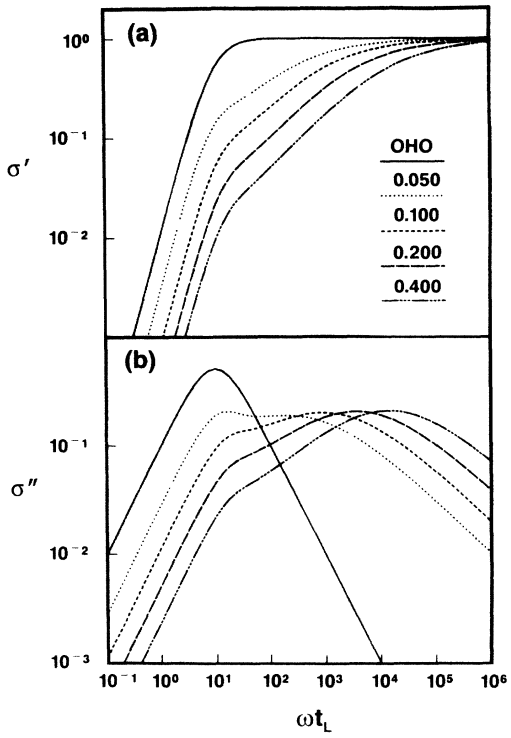

FIG. 4. The real and imaginary parts of the ac conductivity, σ' and σ'', are plotted in (a) and (b), respectively, for the indicated values of L/ξ'.

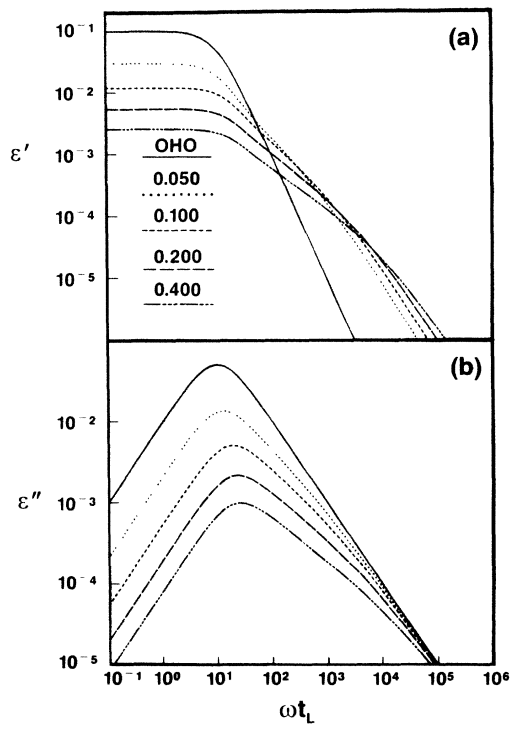

FIG. 5. The real and imaginary parts of the dielectric function, ϵ' and ϵ'', are plotted in (a) and (b), respectively, for the indicated values of L/ξ'.

$$\mathrm{Re}[\sigma(\infty)-\sigma(\omega)]\propto\omega^{-2},\quad \mathrm{Im}[\sigma(\omega)]\propto\omega^{-1}$$
$$\text{for } \omega\gg\omega_c\ . \qquad (18)$$

At ω_c the imaginary parts of σ and ϵ both peak, and the real parts reach half of their maximum values.

For any finite sample size, the response is characteristic of a broad distribution of relaxation times rather than the single relaxation time of an OHO. This distribution of relaxation times directly reflects the distribution of elastic modes of the CDW. The exponents characterizing the frequency dependence of the response are changed from those in Eqs. (17) and (18). In addition, the peaks in ϵ'' and σ'' occur at two different frequencies.

Three different frequency ranges are evident in Figs. 4 and 5. Below ω_L, the cutoff in the phason spectrum, τ^{-1} and K are frequency independent. The response follows that of an OHO with the renormalized τ^{-1}. Above ω_L, τ^{-1} and K vary. A peak is seen in ϵ'' at ω_L, followed by a decrease with apparent exponent near $\frac{1}{2}$. Both σ' and σ'' continue to increase, but at a reduced rate. At a higher frequency, ω_τ, σ'' peaks and σ' reaches about half of its maximum value. For $\omega\gg\omega_\tau$,

$$\mathrm{Re}[\sigma(\infty)-\sigma(\omega)]\propto\omega^{-1/2},\quad \mathrm{Im}[\sigma(\omega)]\propto\omega^{-1/2}\ . \qquad (19)$$

No peak is seen in ϵ'' at ω_τ, just an increase in the rate of falloff with increasing ω.

These features are easily understood in terms of a simple approximation to Eq. (15). The largest frequency-dependent terms in the denominator of Eq. (15) come from $\langle b^-(\omega)\rangle_\alpha$ and $\tilde{K}$. Using the high-frequency form of $\langle b^-\rangle_\alpha$ discussed in Sec. II, we find

$$\sigma(\omega)\simeq[1+\beta(L/\xi')(i\omega)^{-1/2}-i\tilde{K}/\omega]^{-1} \qquad (20)$$

for $\omega>\omega_L$, where $\beta^{-1}=8\pi\eta$.

For $L/\xi'>0.02$, the term from $\langle b^-\rangle_\alpha$ is larger than unity near ω_L and dominates the denominator. Both σ' and σ'' increase roughly as $\omega^{1/2}$ above ω_L. The term from $\tilde{K}$ modifies the effective exponent slightly, but decreases in importance as ω or L/ξ' increase. The constant unity on the right-hand side of Eq. (20) becomes dominant above a frequency ω_τ defined by $|\omega_\tau^{-1}b^-(\omega_\tau)|=1$ [or $\tau^{-1}(\omega_\tau)=1+2^{-1/2}$]. There is a peak in σ'' at ω_τ, and at higher frequencies σ follows Eq. (19). The value of ω_τ is independent of L/ξ', since it only depends on the damping by high-frequency modes. If results for different L/ξ' are plotted in the same units (rather than in terms of ω_L), the peaks in σ'' lie on top of each other.

For very small samples, $L/\xi'<0.02$, $\omega_\tau<\omega_L$, and τ^{-1} is never much larger than 1. The term from $\tilde{K}$ becomes important and σ'' and ϵ'' peak at $\omega_c=\tilde{K}\tau^{-1}(0)$. The response follows that of an OHO until $\omega\gg\omega_L>\omega_c$, where there is a smooth crossover from the high-frequency behavior of an OHO, Eq. (18), to Eq. (19).

In terms of a distribution of relaxation times $g(\tilde{\tau})$,

$$\epsilon''(\omega)=\int d\tilde{\tau}\,g(\tilde{\tau})\omega\tilde{\tau}/[1+(\omega\tilde{\tau})^2]\ . \qquad (21)$$

Thus ϵ'' follows $g(\tilde{\tau})$, but is broadened by a Lorentzian. The distribution of relaxation times represented in $\langle b^-\rangle_\alpha$ is zero for $\tilde{\tau}\gg\omega_L^{-1}$, peaks for $\tilde{\tau}\simeq\omega_L^{-1}$, and varies roughly as $\tilde{\tau}^{1/2}$ for $\tilde{\tau}\ll\omega_L^{-1}$. The form of ϵ'' in Fig. 5 reflects this behavior, peaking near ω_L and falling off like an OHO at low frequencies and with an apparent exponent near $-\frac{1}{2}$ at high frequencies. No separate relaxation time associated with ω_τ is seen. An OHO would show a single relaxation process centered at ω_c. For the values of L/ξ' in Figs. 4 and 5, ω_c is slightly larger than ω_L and contributes to the peak in ϵ'' near ω_L.

A common way of illustrating a distribution of relaxation times is a Cole-Cole[29] plot of ϵ' vs ϵ'' (Fig. 6). For a single relaxation time (OHO) the plot gives a semicircle. For a distribution of relaxation times the curve lies below the semicircle. An asymmetric plot implies an asymmetric distribution of relaxation times. The existence of two peaks in the plot indicates two classes of relaxation processes. Our results (Fig. 6) are indicative of a single relaxation process with a broad asymmetric distribution of relaxation times.

In the GZC model with a sinusoidal potential, the peaks in ϵ'' and σ'' both shift to lower frequency as the dc bias, $\tilde{E}$, increases towards E_T. Both depend on $\tilde{K}$, which decreases with increasing $\tilde{E}$ as the curvature of the effective potential near the stable phase $\tilde{\Delta}$ decreases. For a single sine-wave potential, $\tilde{K}\propto\cos(\sin^{-1}|\tilde{E}/E_T|)$. For any periodic force with quadratic extrema, $\tilde{K}\propto(E_T-\tilde{E})^{1/2}$ near E_T.

If there is a distribution of relaxation times, the peaks in ϵ'' and σ'' need not shift together as $\tilde{K}$ changes. In our calculation $\tilde{K}$ determines ω_c and the peak in ϵ'' shifts with ω_c as $\tilde{E}$ increases. In contrast, the peak in σ'' and the rapid rise in σ' do not shift appreciably. They are determined by the decrease of τ^{-1} and remain near ω_τ. Figure 7 illustrates this behavior for $L/\xi'=0.2$ and a bias of about $0.995E_T$, where $\tilde{K}$ has decreased by a factor of 10 from its value at zero bias. The Cole-Cole plot continues to show a single peak.

There have been a large number of experimental studies of the ac response in recent years.[4,18,30–35] The response is found[32–34] to be nonlinear in the ac amplitude for fields greater than a few percent of E_T. The linear response generally shows two characteristic frequencies,[4,31–35] just as in our calculation. At one frequency there is a sharp

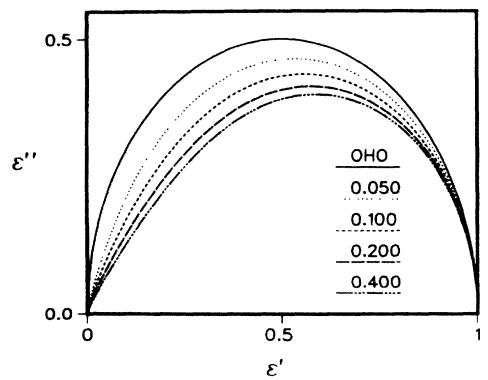

FIG. 6. A Cole-Cole plot of ϵ'' vs ϵ' [normalized to $\epsilon'(0)$] for the indicated values of L/ξ', which illustrates the broad distribution of relaxation times.

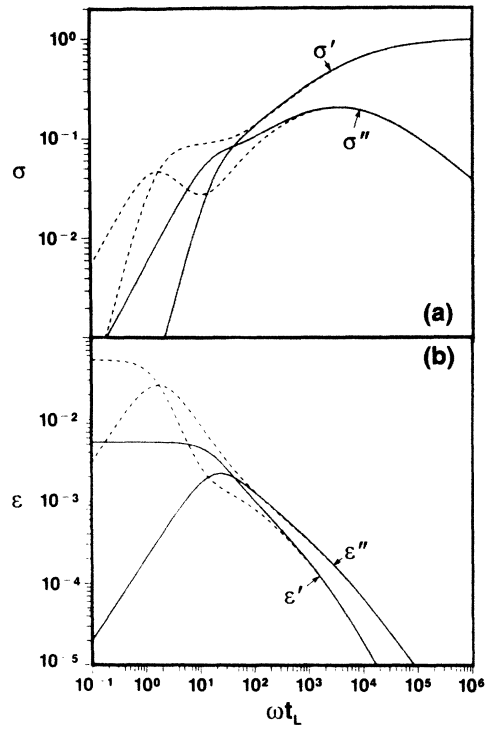

FIG. 7. (a) Conductivity and (b) dielectric function calculated for a sample with $L/\xi'=0.2$ at two different dc biases: 0 (solid lines) and $0.995E_T$ (dashed lines).

rise in the value of σ' (in a linear plot) and σ'' reaches a maximum. Based on the rigid CDW model, this frequency has been interpreted as ω_c and used to determine the effective force constant $\tilde{K}$ of the periodic potential.[3,17] Our results suggest a different interpretation, i.e., that this frequency corresponds to ω_τ. Recent measurements[4,31–35] show a maximum in ϵ'' at a lower frequency. We would interpret this frequency as ω_c or ω_L, which we expect to be of the same order in infinite samples.

Cava *et al.*[4] were the first to find this peak in ϵ'' and to analyze it in terms of a distribution of relaxation times. For $K_{0.3}MoO_3$, they found that the variation of the peak position with temperature fitted an Arrhenius law. Above the peak, the frequency dependence of ϵ'' was described by a temperature-independent exponent of 0.70, which is very close to the apparent exponent seen in our curves. The exponent characterizing the response below the peak was very temperature dependent. Similar results[33–35] have been reported in TaS_3.

These measurements are presumably on samples where $L/\xi' \gg 1$. As discussed above and elsewhere,[9,26,36] in the limit $L/\xi' \to \infty$ the cutoff in the phason spectrum ω_L saturates at a finite value. The distribution of relaxation times near this peak will depend on the details of the distribution of phason modes and may differ from the form found in our calculation. Since relaxation via these modes is not thermally activated, the shape of $g(\tilde{\tau})$ for $\tilde{\tau} < \omega_L^{-1}$ will not vary with temperature. This is consistent with experimental results.[4] While experiments show that the position of ω_L does vary with temperature, many other quantities, such as the threshold field, static dielectric constant, normal resistance τ_0^{-1}, and CDW amplitude, are also temperature dependent.

The observed distribution of relaxation times at long times, $\tilde{\tau} > \omega_L^{-1}$, can be understood in terms of thermally activated processes. For $L > \xi'$ there are many metastable states[36] of the CDW corresponding to variations in ϕ over lengths of order ξ. These cannot be described by our perturbation theory. Thermal excitations between these metastable states will also contribute to the ac conductivity. The characteristic relaxation times are determined by the temperature and the barrier heights. For a fixed distribution of barrier heights, the distribution of relaxation times broadens as the temperature is lowered. This is consistent with the observed broadening of $g(\tilde{\tau})$ at large $\tilde{\tau}$ as T is decreased[4] in $K_{0.3}MoO_3$.

An alternative explanation for the data on $K_{0.3}MoO_3$ is that the peak observed in ϵ'' results from a peaked distribution of relaxation times, all of which represent thermally activated processes. The activated shift in ω_L with temperature is then understood. However, there are several problems with this interpretation. The first is that it provides no explanation for the asymmetric broadening of $g(\tilde{\tau})$ as T decreases. A more important problem is that one would expect to see another peak in $\epsilon''(\omega)$ corresponding to the nonactivated motion of the CDW about a single locally stable configuration, which is described by our calculation. However, experiments which extend to a few GHz, where inertial effects become important, show no second peak.[18,31] Our model naturally explains these observations.

There are two ways of testing these models experimentally. The first is to study the response as a function of bias. In our calculation the peak in ϵ'' is associated with ω_c and shifts to lower frequency as the bias increases and $\tilde{K}$ decreases. The peak in σ'' does not shift since it is determined by high-frequency modes. Previous measurements are consistent with these predictions. The frequency at which σ'' peaks appears to be bias independent.[3,4] Cava *et al.*[4] present data for ϵ at two fields, 0 and $0.77E_T$, which indicate that the peak in ϵ'' shifts to lower frequencies with increasing bias. If the peak in ϵ'' were thermally activated and increasing the bias lowered the effective barriers, the peak would shift in the opposite direction.

Another test of the two explanations of the peak in ϵ'' involves studies of response as a function of sample size. The distribution of metastable states should depend on the sample size. In particular, we suggest that in samples with kinked dV/dI characteristics there will be few if any metastable states, and that the low-frequency response will approach that of an OHO.

IV. SUMMARY AND CONCLUSIONS

We have shown that a detailed study of the CDW dynamics in samples of dimension $L < \xi'$ provides a coherent explanation for many features of the observed dc and ac conductivities of CDW conductors. The deformability of the CDW condensate plays the central role in these results. As the CDW moves in response to an applied ac or dc field, it deforms. Elastic modes of the

CDW are excited which damp the motion. The level of excitation and the resulting damping depend on the ratio of the characteristic frequency of the mode to that of the motion: the ac frequency or the narrow-band noise frequency.[1] The total effective damping rate varies with frequency and current in the same way.

Response at high frequencies and currents is only affected by high-frequency modes. The spectrum of these modes is not affected by finite sample size or impurity pinning. The asymptotic high-field behavior of the dc conductivity derived by SCF and the leading correction to it (Fig. 3) are determined by these high-frequency modes. They also determine the high-frequency form of the ac conductivity [Eq. (19)].

At lower frequencies and currents the spectrum is altered by both finite sample size and impurity pinning. The perturbation theory used here is only accurate when the effects of impurity pinning are small, i.e., for sufficiently high frequencies or for sufficiently small samples. The main effect of sample size in small samples ($L \ll \xi'$) is to introduce a low-frequency cutoff ω_L in the spectrum of elastic modes or phasons. This introduces a kink in dV/dI at the dc threshold whose width decreases with increasing sample size (Fig. 2). The distribution of relaxation times seen in the ac response (Fig. 5) is cut off at ω_L. Above ω_L, a broad distribution of relaxation times corresponding to the distribution of phasons is seen. Measurements on samples with $L/\xi' \ll 1$ should show all of these features. Recent advances in growing ultrapure samples,[37] where ξ is large, may facilitate such experiments.

In infinite samples, impurity pinning will also introduce a cutoff frequency in the phason spectrum at dc biases below threshold. While the form of the spectrum near this cutoff may not be the same as that near ω_L in a small sample, the resulting ac response will show the same qualitative features. In particular, the imaginary part of the dielectric function ϵ'' will peak at the cutoff frequency, which will, in general, be different from the frequency where the imaginary part of the conductivity peaks. The form of ϵ'' will reflect the distribution of modes. Changes in dc bias will shift the peak in ϵ'' while the peak in σ'' will remain fixed. We expect the largest differences from our results to occur below the cutoff frequency, where the spectrum of modes in a sample with $L \ll \xi'$ is identically zero, while the spectrum of an infinite sample may exhibit a long tail.[26,36] Infinite samples will also contain many metastable states.[26,36] Thermally activated transitions between these states will lead to another contribution to the ac response which is not present in small samples.

As the threshold field is approached, the cutoff frequency in infinite samples will go to zero. The new low-frequency modes necessarily correspond to lengths much greater than the static phase coherence length ξ. Scaling approaches[26,27] are required to treat these length scales properly; they cannot be described by the perturbation approach used here. However, a qualitative picture of the effect of these low-frequency modes on the dc response near threshold can be obtained by a naive extrapolation of our results for the form of the damping by high-frequency modes to low frequencies. The low-frequency modes remove the kink in dV/dI near threshold which is found for finite samples (Fig. 2). The current-voltage relation becomes $I \propto (E - E_T)^{3/2}$. While the same exponent is found in Fisher's mean-field scaling theory,[26] the agreement is coincidental. Experimental measurements find[15,24,25] a variety of apparent exponents from $\frac{1}{2}$ (which leads to a kink in dV/dI) to 4. Our calculation suggests that this may reflect a change in sample size. Experiments are needed to examine this point.

The results described above are for steady-state measurements. The integration over past times in Eq. (2) naturally introduces memory effects, which lead to interesting transient behavior. We find hysteresis loops in the I-V characteristic when the applied field is cycled rapidly,[7] response to current pulses that depends on the direction of the previous pulses,[7,8] and a number of other effects. In each case the times over which these effects occur are of order t_L. Based on the observed peak in σ'' for $NbSe_3$ and the ratio of ω_τ to t_L^{-1} for a sample with $L/\xi' = 0.1$ (Fig. 4), this should correspond to times of order 20 μs. Some experiments[6-8] find memory effects and hysteresis for timescales of seconds or longer.[38] This indicates that the samples contain many Lee-Rice domains and that metastable processes enter which are not described by our perturbation technique.

In our calculation transient effects have two major origins. If $\Delta(t)$ is replaced with its Taylor expansion in Eq. (2), one finds inertial terms. For $L < \xi'$ the system remains underdamped, but the effective mass increases with L/ξ', leading to more pronounced transient effects. A related effect is that the effective periodic force varies as a function of current and frequency. The amplitude of the second Fourier component of the force is $\int B^+(t)dt$ in the static limit. For finite current it decreases as $b^+(\dot{\Delta})$ ($\propto \dot{\Delta}^{-1/4}$ for large $\dot{\Delta}$). Higher Fourier components decrease even faster. Thus the effective pinning force depends on current. An analogous phenomenon is the difference between static and sliding coefficients of friction in normal systems. If the magnitude of the effective pinning force decreases sufficiently rapidly, the static I-V characteristic may become hysteretic. This does not happen for $L < \xi'$, but the current dependence of the pinning force does contribute to the strong transient behavior.

The results presented above illustrate the importance of deformations of the CDW on length scales less than ξ. These have not yet been included in the scaling treatments[26,27] developed for longer length scales. A complete understanding of CDW dynamics requires a unification of these two approaches. Future work should also consider the effect of temperature, which appears to play an important role in many experiments.[4,5,25,31-35,38]

ACKNOWLEDGMENTS

We thank J. P. Stokes, G. Grüner, and A. Zettl for providing unpublished experimental data and J. R. Schrieffer, A. N. Bloch, S. Bhattacharya, S. Coppersmith, G. Grüner, J. P. Stokes, and A. Zettl for useful conversations.

APPENDIX

To evaluate the linear response, we decompose Δ into a static component $\tilde{\Delta}$ and a small time-dependent part $d(t)$. The static component must satisfy

$$0=\tilde{F}+\mathrm{Im}\left[Ae^{i\tilde{\Delta}}+e^{2i\tilde{\Delta}}\int dt' B^{+}(t-t')\right], \tag{A1}$$

where $\tilde{F}$ is the normalized dc field. The force constant $\tilde{K}$ for small static displacements about $\tilde{\Delta}$ is

$$\tilde{K}=\frac{\partial\tilde{F}}{\partial\tilde{\Delta}}=-\mathrm{Re}\left[Ae^{i\tilde{\Delta}}+2e^{2i\tilde{\Delta}}\int dt' B^{+}(t-t')\right]. \tag{A2}$$

Expanding Eq. (7) to first order in d and using Eqs. (A1) and (A2), we find

$$\frac{\partial d(t)}{\partial t}=f(t)-\tilde{K}d(t)+\int dt'[d(t')-d(t)]\times\mathrm{Re}[e^{2i\tilde{\Delta}}B^{+}(t-t')+B^{-}(t-t')], \tag{A3}$$

where f is the ac component of the applied field. Taking the Fourier transform gives

$$f(\omega)=i\omega d(\omega)+\tilde{K}d(\omega)+d(\omega)[b^{+}(\tilde{\Delta},0)+b^{-}(0)-b^{+}(\tilde{\Delta},\omega)-b^{-}(\omega)], \tag{A4}$$

where $b^{+}(\tilde{\Delta},\omega)$ is the Fourier transform of $\mathrm{Re}[\exp(2i\tilde{\Delta})B^{+}(t)]$ and $b^{-}(\omega)$ is the Fourier transform of $B^{-}(t)$.

The linear response is

$$\sigma(\omega)=\frac{i\omega d(\omega)}{f(\omega)}=\{1-(i/\omega)[\tilde{K}+b^{+}(\tilde{\Delta},0)+b^{-}(0)-b^{+}(\tilde{\Delta},\omega)-b^{-}(\omega)]\}^{-1}. \tag{A5}$$

Using the definition of τ^{-1} [Eq. (14)], we can rewrite Eq. (A5) as Eqs. (15) and (16).

---

*Present address: Department of Physics and Astronomy, Johns Hopkins University, Baltimore, MD 21218.

† Present address: Department of Physics, University of California—San Diego, La Jolla, CA 92093.

[1]For an overview, see *Charge Density Waves in Solids,* Proceedings of the International Conference, Budapest, Hungary, 1985, Vol. 217 of *Lecture Notes in Physics*, edited by Gy. Hutiray and J. Solyóm (Springer-Verlag, New York, 1985).

[2]R. M. Fleming and C. C. Grimes, Phys. Rev. Lett. **42**, 1423 (1979).

[3]G. Grüner, A. Zettl, W. G. Clark, and J. Bardeen, Phys. Rev. B **24**, 7247 (1981).

[4]R. Cava, R. M. Fleming, P. Littlewood, E. A. Rietman, L. F. Schneemeyer, and R. G. Dunn, Phys. Rev. B **30**, 757 (1984).

[5]S. Bhattacharya, J. P. Stokes, M. O. Robbins, and R. A. Klemm, Phys. Rev. Lett. **54**, 2453 (1985).

[6]A. Zettl and G. Grüner, Phys. Rev. B **26**, 2298 (1982); J. Dumas, C. Schlenker, J. Marcus, and R. Buder, Phys. Rev. Lett. **50**, 757 (1983).

[7]R. M. Fleming and L. F. Schneemeyer, Phys. Rev. B **23**, 6996 (1983).

[8]J. C. Gill, Solid State Commun. **39**, 1203 (1981).

[9]H. Fukuyama and P. A. Lee, Phys. Rev. B **17**, 535 (1978); **18**, 6245 (1978); P. A. Lee and T. M. Rice, *ibid.* **19**, 3970 (1979).

[10]K. B. Efetov and A. I. Larkin, Zh. Eksp. Teor. Fiz. **72**, 2350 (1977) [Sov. Phys.—JETP **45**, 1236 (1977)].

[11]R. A. Klemm and J. R. Schrieffer, Phys. Rev. Lett. **51**, 47 (1983); Synth. Met. **11**, 307 (1985).

[12]J. Bardeen, Phys. Rev. Lett. **42**, 1498 (1979); **45**, 1978 (1980); **55**, 1010 (1985); R. E. Thorne, J. H. Miller, Jr., W. G. Lyons, J. W. Lyding, and J. R. Tucker, *ibid.* **55**, 1006 (1985).

[13]L. Sneddon, M. C. Cross, and D. S. Fisher, Phys. Rev. Lett. **49**, 292 (1982).

[14]L. Sneddon, Phys. Rev. B **29**, 719 (1984).

[15]P. Monceau, J. Richard, and M. Renard, Phys. Rev. B **25**, 931 (1982).

[16]R. M. Fleming, D. E. Moncton, and D. B. McWhan, Phys. Rev. B **18**, 5560 (1978).

[17]G. Grüner, A. Zawadowski, and P. M. Chaikin, Phys. Rev. Lett. **46**, 511 (1981).

[18]Recent results show inertial effects may become important above a few GHz: S. Sridhar, D. Reagor, and G. Grüner, Phys. Rev. Lett. **55**, 1196 (1985).

[19]Damping by phonon scattering is considered in S. Takada, K. Y. M. Wong, and T. Holstein, Phys. Rev. B **32**, 4639 (1985). Damping by electron scattering is treated by W. L. McMillan, Phys. Rev. B **12**, 1197 (1976). These mechanisms are frequency independent at frequencies below the Debye and plasma frequencies, respectively. Inertial terms become important at much lower frequencies (Ref. 18).

[20]J. P. Stokes (private communication).

[21]Kinsel has found a kink to be a universal feature of a very different model. The model also predicts an activated temperature dependence of the CDW current which is not observed. W. Kinzel, Phys. Rev. Lett. **51**, 1787 (1983).

[22]A. Zettl and G. Grüner (private communication).

[23]J. B. Sokoloff, Phys. Rev. B **23**, 1992 (1981).

[24]P. Monceau, M. Renard, J. Richard, M. C. Saint-Lager, and Z. Z. Wang, in *Charge Density Waves in Solids,* Ref. 1, p. 279. Note that these exponents were obtained from the narrow-band noise frequency and recent work suggests that this does not scale linearly with I_{CDW} [S. E. Brown and G. Grüner, Phys. Rev. B **31**, 8392 (1985)].

[25]M. O. Robbins, J. P. Stokes, and S. Bhattacharya, Phys. Rev. Lett. **55**, 2822 (1985).

[26]D. S. Fisher, Phys. Rev. Lett. 50, 1486 (1983); Phys. Rev. B **31**, 1396 (1985).

[27]R. K. Ritala and J. A. Hertz, NORDITA Report No. 85-14 (unpublished).

[28]As $L/\xi'\to 0$, $\omega_c t_L\sim(L/\eta\xi')^{1/2}$ goes to zero. The curves labeled OHO in Figs. 4 and 5 correspond to $\omega_c t_L=10$, but have the same form as the response in the limit $L/\xi'\to 0$.

[29]K. S. Cole and R. H. Cole, J. Chem. Phys. **9**, 341 (1941).

[30]W. Wu, L. Mihaly, G. Mozurkewich, and G. Grüner, Phys. Rev. Lett. **52**, 2382 (1984).

[31]R. P. Hall, M. Sherwin, and A. Zettl, in *Charge Density Waves*

in Solids, Ref. 1, p. 314.
[32]R. J. Cava, R. M. Fleming, R. G. Dunn, E. A. Rietman, and L. F. Schneemeyer, Phys. Rev. B **30**, 7290 (1984).
[33]R. J. Cava, R. M. Fleming, R. G. Dunn, and E. A. Rietman, Phys. Rev. B **31**, 8325 (1985).
[34]J. P. Stokes, M. O. Robbins, and S. Bhattacharya, Phys. Rev. B **32**, 6939 (1985).
[35]C. B. Kalem, N. P. Ong, and J. C. Eckert (unpublished).
[36]P. Littlewood, in *Charge Density Waves in Solids,* Ref. 1, pp. 369—376, and unpublished.
[37]R. V. Coleman (private communication).
[38]R. J. Cava, R. M. Fleming, E. A. Rietman, R. G. Dunn, and L. F. Schneemeyer, Phys. Rev. Lett. **53**, 1677 (1984).